MADRID
inter.noise 2019
June 16 - 19
NOISE CONTROL FOR A BETTER ENVIRONMENT

Railway rolling noise minimization by topology optimization techniques using the mixed FE formulation

Ferrándiz, B.[1]; Nadal, E.[2]; Martínez-Casas, J.[3]; Denia, F.D.[4]; Ródenas, J.J.[5]
Centro de Investigación en Ingeniería Mecánica, Universitat Politècnica de València
Camino de Vera s/n, 46022 Valencia, Spain

ABSTRACT

Railway rolling noise limits the use of higher speed trains near cities. Several methods to address this problem can be found in the literature, such as the modification of the wheel web geometry, or the use of perforations. In this work, the authors propose the design of an acoustic optimized train fairing. This will be obtained via a gradient-based Topology Optimization (TO) process, utilized to minimize the mean acoustic pressure amplitude within a domain surrounding the wheel.

In order to construct the acoustic optimized topology of the train fairing, a mixed Finite Element (FE) formulation (displacement/pressure) is implemented. This formulation is suitable to be used under the TO framework since it does not require the explicit representation of the boundary of the structure in order to solve the coupled vibro-acoustic problem. However, due to its high computational cost, the authors propose the use of the mixed formulation combined with the Helmholtz equation formulated in terms of pressure, in order to obtain an agile TO algorithm in the framework of the fluid-structure coupled problems. This method is then applied to the design of a bogie fairing, in order to minimize the acoustic pressure amplitude within the target domain.

Keywords: Mixed formulation, domain decomposition, wheel fairing
I-INCE Classification of Subject Number: 31

1. INTRODUCTION

Density-based Topology Optimization (TO) [1] has been successfully applied to elasticity design problems [2]. This method has proved to be an effective way to

[1]borferca@upvnet.upv.es
[2]ennaso@upvnet.upv.es
[3]jomarc12@mcm.upv.es
[4]fdenia@mcm.upv.es
[5]jjrodena@mcm.upv.es

distribute material efficiently in order to obtain designs with reduced mass, while minimizing an objective function, e.g. strain energy under a specific load case. The TO methodology replaces the concept of shape by the density layout of the elements contained in the design space $\mathbf{x}$, which is to be optimized. Hence, not only the maximum value ($x_e = 1$ for hard material element), but also the intermediate values contribute with fictitious mechanical properties.

However, for vibro-acoustics problems, the equation to solve is different for the structure and air domains, and the exact location of the coupling boundary between them is required. This makes the density-based approach unsuitable for this and other kinds of multi-physics problems.

This difficulty can be overcome following several strategies. Some studies disregard the effect of the acoustic perturbation on the structure; only the acoustic wave equation is solved, hence decoupling the problem. In [3], a horn-lens configuration is optimized by TO in order to minimize the amplitude of the reflected wave into the waveguide, whereas in [4] the ceiling of a room is topologically optimized in order to reduce noise at a target location. The elasticity of the structure is also not taken into account in [5], in order to design a topologically optimized noise barrier placed between an emitter and a receiver location where sound pressure is to be minimized.

Other studies focus on the TO of inner structural components of the design domain, rather than modifying the coupling interface. Hence, the coupled system is solved. In [6], an enclosure is stiffened by TO in order to reduce low frequency noise in the interior. In [7] a bi-material surface is optimized in order to reduce the sound power radiated under certain load cases, whereas in [8] the structure attached to the shell of a hearing instrument is optimized topologically in order to minimize the sound pressure at certain microphone locations.

If the air-structure interface is to be modified, the two phase material model has to be used along with evolutionary algorithms. The level-set method [9] and the bi-directional evolutionary structural optimization (BESO) [10] have been proved to be good alternatives to optimize sound barriers while solving the acoustic field and the linear elasticity of the structure. However, the solution reached by these methods often depends on the initial guess design, which can be difficult to obtain in complex problems involving multi-physics coupling.

Finally, a change in the formulation is proposed by some authors in order to solve the coupled problem. In [11, 12], the displacement/pressure (u/p) mixed formulation [13] is adopted to solve static and harmonic fluid-structure problems, and carry out the TO of shells and sound barriers, respectively. Therefore, the authors of this work propose to limit the use of this computationally-expensive formulation to a small region of the domain (where the noise barrier is designed), whereas the rest of the acoustic domain is solved using the standard pressure Helmholtz equation. As coupling conditions between both subdomains, the kinematic compatibility and elastic equilibrium at the interface are considered. The method is then applied to the design of a lower train fairing, and a multi-objective function is constructed in order to minimize the sound pressure at a target location, as well as the strain energy under a static load case.

2. THE FLUID-STRUCTURE PROBLEM

Figure 1 shows the problem set-up mentioned in Section 1. The domain is decomposed into two subdomains: the acoustic domain Ω_a, where the Helmholtz equation is solved

in terms of pressure, and the design domain Ω_d where the u/p formulation is adopted. Γ_a and Γ_d are the corresponding problem boundaries, whereas Γ_{coup} is the coupling interface between Ω_a and Ω_d. The area of design of the sound barrier is represented in Figure 1 in dark grey, whereas the area where sound amplitude is to be minimized, Ω_i is coloured in light grey. The wheel geometry [14] is denoted by Γ_{rad}, and excitation of the acoustic field is carried out by means of a displacement input. Finally, Γ_{abs} is modelled as an absorbent wall in order to avoid wave reflections.

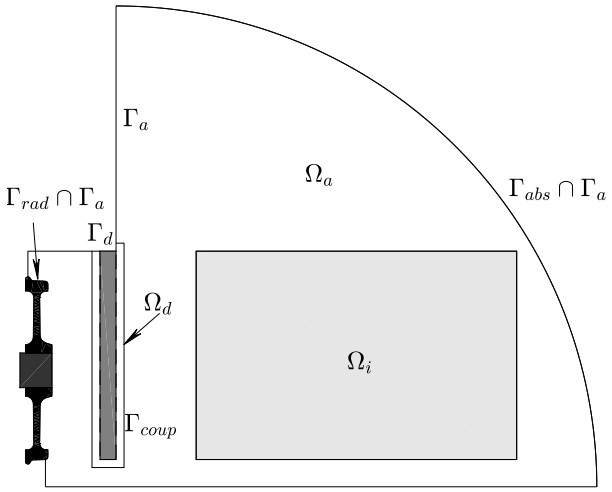

Figure 1: Problem scheme.

The aim of this study is to carry out the TO of a thin wheel fairing, in order to minimize the sound pressure amplitude integral within Ω_i. Note that some elements within Ω_d do not participate in the TO process and their design variable is fixed $x_e = 0$ (air) at all stages of the optimization, as it will be explained in Section 2.4.

2.1. Material interpolation model

Gradient-based TO methods require a continuous and differentiable material model, so that material properties range from those of the air (for elements with $x_e = 0$) to those of the solid structure (for elements with $x_e = 1$).

As suggested by Yoon *et al.* [12], both air and solid vibro-acoustic properties can be described using the bulk and shear moduli, denoted by K and G respectively, and density ρ. For the solid material, K_s and G_s are related to the Young's modulus E and Poisson ratio ν. For the two-dimensional plane strain case [12]:

$$K_s = \frac{E}{2(1+\nu)(1-2\nu)}\,, \tag{1}$$

$$G_s = \frac{E}{2(1+\nu)}\,, \tag{2}$$

while air has a bulk modulus related to its density and speed of sound c_a, and null shear modulus [12]:

$$K_a = \rho_a c_a^2\,, \tag{3}$$

$$G_a = 0\,. \tag{4}$$

The rational approximation of material properties (RAMP) [12] is used in this work to interpolate the material properties from those of the air to those of the solid, while penalizing intermediate values of x_e. This can be stated as [12]:

$$K(x_e) = K_s \frac{x_e}{1+(1-x_e)n} + K_a \left(1 - \frac{x_e}{1+(1-x_e)n}\right) , \tag{5}$$

$$G(x_e) = G_s \frac{x_e}{1+(1-x_e)n} , \tag{6}$$

$$\rho(x_e) = \rho_s x_e + \rho_a (1-x_e) . \tag{7}$$

2.2. The mixed formulation

As mentioned in Section 1, the u/p mixed formulation [13] allows to solve the vibro-acoustic problem without the need to define the coupling interface. Next, the governing equations for Ω_d are recalled. By applying the Newton's second law to a control volume in any continuum, and neglecting the body force term, the following expression is obtained [13]:

$$\nabla \cdot \hat{\boldsymbol{\sigma}} = \rho \frac{\partial^2 \hat{\mathbf{u}}}{\partial t^2} , \tag{8}$$

$\hat{\boldsymbol{\sigma}}$ and $\hat{\mathbf{u}}$ being the stress tensor and the displacement vector. By assuming a time-harmonic solution of the stress and displacement fields, with angular frequency ω so that $\hat{\boldsymbol{\sigma}} = \boldsymbol{\sigma} e^{j\omega t}$ and $\hat{\mathbf{u}} = \mathbf{u} e^{j\omega t}$, the following expression is obtained [12]:

$$\nabla \cdot \boldsymbol{\sigma} = -\omega^2 \rho \mathbf{u} . \tag{9}$$

The stress tensor can be decomposed into its volumetric and deviatoric components:

$$\boldsymbol{\sigma} = K \varepsilon_v \boldsymbol{\delta} + 2G\mathbf{e} , \tag{10}$$

ε_v and $\mathbf{e}$ being the volumetric and deviatoric strains, and $\boldsymbol{\delta}$ being the Kronecker's delta. The bulk modulus K and shear modulus G will be used in this article to characterize both the air and structure [12]. The volumetric strain is defined as:

$$\varepsilon_v = \frac{\Delta V}{V} = \varepsilon_{xx} + \varepsilon_{yy} = \mathbf{m}^T \boldsymbol{\varepsilon} , \tag{11}$$

where the strain tensor is $\boldsymbol{\varepsilon} = \left\{\varepsilon_{xx}, \varepsilon_{yy}, \varepsilon_{xy}\right\}^T$, and $\mathbf{m} = \left\{1, 1, 0\right\}^T$. As an alternative to the pure displacement formulation, one may include the pressure p as a variable [13]:

$$p = -K\varepsilon_v = -K \nabla \cdot \mathbf{u} , \tag{12}$$

whereas the deviatoric strain in 2D can be calculated as:

$$\mathbf{e} = \boldsymbol{\varepsilon} - \frac{\varepsilon_v}{2} = \mathbf{D}_d \, \boldsymbol{\varepsilon} , \tag{13}$$

where $\mathbf{D}_d = I_0 - 1/2 \, \mathbf{m}^T \mathbf{m}$, and I_0 is the diagonal matrix. The weak form of Equations 9 and 10 can be stated as:

$$\int_{\Omega_d} \delta\boldsymbol{\varepsilon}^T 2G\mathbf{e} \, \mathrm{d}\Omega - \int_{\Omega_d} \delta\boldsymbol{\varepsilon}^T \left(p\boldsymbol{\delta}\right) \, \mathrm{d}\Omega - \omega^2 \int_{\Omega_d} \delta\mathbf{u}^T \mathbf{u} \, \mathrm{d}\Omega - \int_{\Gamma_d} \delta\mathbf{u}^T \left(\boldsymbol{\sigma}\mathbf{n}_u\right) \, \mathrm{d}\Omega = 0 , \tag{14}$$

$\mathbf{n}_u$ being the outward unit vector normal to the boundary. Taking into account Equations 11 and 13, it yields:

$$\int_{\Omega_d} \delta\boldsymbol{\varepsilon}^T 2G\mathbf{D_d}\boldsymbol{\varepsilon}\,\mathrm{d}\Omega - \int_{\Omega_d} \delta\boldsymbol{\varepsilon}^T \mathbf{m}p\,\mathrm{d}\Omega - \omega^2 \int_{\Omega_d} \delta\mathbf{u}^T\mathbf{u}\,\mathrm{d}\Omega - \int_{\Gamma_d} \delta\mathbf{u}^T\,(\boldsymbol{\sigma}\mathbf{n}_u)\;\mathrm{d}\Omega = 0\,. \tag{15}$$

Additionally, the weak form of Equation 12 is:

$$\int_{\Omega_d} \delta p\left(p/K + \mathbf{m}^T\boldsymbol{\varepsilon}\right)\,\mathrm{d}\Omega = 0\,. \tag{16}$$

The FEM is applied to Equations 15 and 16, and in order to fulfill the Inf-Sup condition [13], the domain is meshed with quadrilateral elements using second and first order nodal shape functions $\mathbf{N_u}$ and $\mathbf{N_p}$ for displacements and pressure, respectively.

The following system of equations (expressed here in compact form) is obtained [2, 12, 13]:

$$\begin{bmatrix} \mathbf{K}_{uu} - \omega^2\mathbf{M}_{uu} & \mathbf{C}_{up} \\ \mathbf{C}_{up}^T & \mathbf{D}_{pp} \end{bmatrix} \begin{bmatrix} \tilde{\mathbf{U}} \\ \tilde{\mathbf{P}} \end{bmatrix} = \begin{bmatrix} \mathbf{F}_u \\ 0 \end{bmatrix}\,, \tag{17}$$

where $\tilde{\mathbf{U}}$ and $\tilde{\mathbf{P}}$ are the nodal values of displacements and pressure. For the full derivation of the mixed formulation, the reader is referred to references [11–13]. The expressions of the global matrices contained in Equation 17 are:

$$\mathbf{K}_{uu} = \sum_{e=1}^{N_d} 2G_e \int_{\Omega_e} \mathbf{B}_u^T\mathbf{D}_d\mathbf{B}_u\,\mathrm{d}\Omega\,, \tag{18}$$

$$\mathbf{M}_{uu} = \sum_{e=1}^{N_d} \rho_e \int_{\Omega_e} \mathbf{N}_u^T\mathbf{N}_u\,\mathrm{d}\Omega\,, \tag{19}$$

$$\mathbf{C}_{up} = \sum_{e=1}^{N_d} -\int_{\Omega_e} \mathbf{B}_u^T\mathbf{m}\mathbf{N}_p\,\mathrm{d}\Omega\,, \tag{20}$$

$$\mathbf{D}_{pp} = \sum_{e=1}^{N_d} -\frac{1}{K_e}\int_{\Omega_e} \mathbf{N}_p^T\mathbf{N}_p\,\mathrm{d}\Omega\,, \tag{21}$$

$$\mathbf{F}_u = \sum_{e=1}^{N_d} \int_{\Gamma_e\cap\Gamma_d} \mathbf{N}_u^T\,(\boldsymbol{\sigma}\mathbf{n}_u)\;\mathrm{d}\Gamma\,, \tag{22}$$

where $\mathbf{B_u}$ is the usual strain-displacement matrix, and N_d is the number of elements in the design space.

2.3. Helmholtz equation

The sound propagation in the homogeneous medium corresponding to Ω_a can be described by the following version of the Helmholtz equation:

$$\nabla^2 p + \frac{\omega^2}{c_a^2}p = 0\,, \tag{23}$$

where c_a is the speed of sound. The FEM is applied in an analogous way to Section 2.2, obtaining [15]:

$$\left(\mathbf{K}_a - \omega^2\mathbf{M}_a\right)\tilde{\mathbf{P}}_a = \mathbf{F}_a\,, \tag{24}$$

$\tilde{\mathbf{P}}_a$ being the pressure value at the nodes of Ω_a. The stiffness, mass and force terms are:

$$\mathbf{K}_a = \sum_{e=1}^{N_a} \int_{\Omega_e} \mathbf{B}_p^T \mathbf{B}_p \, \mathrm{d}\Omega \,, \tag{25}$$

$$\mathbf{M}_a = \frac{1}{c_a^2} \sum_{e=1}^{N_a} \int_{\Omega_e} \mathbf{N}_p^T \mathbf{N}_p \, \mathrm{d}\Omega \,, \tag{26}$$

$$\mathbf{F}_a = \sum_{e=1}^{N_a} \int_{\Gamma_e \cap \Gamma_a} \mathbf{N}_p^T \frac{\partial p}{\partial n_p} \, \mathrm{d}\Gamma \,, \tag{27}$$

where N_d is the number of elements out of the design domain, $\mathbf{n}_p$ is the outward unit vector normal to the boundary, and $\mathbf{B}_p = \nabla \mathbf{N}_p$.

2.4. Subdomain coupling

The Helmholtz equation can be derived from the u/p formulation when the air properties are assigned ($G_a = 0$, $K_a = \rho_a c_a^2$) to the governing and the constitutive equations. Equations 9 and 12 can be simplified as follows [12]:

$$\nabla p - \omega^2 \rho_a \mathbf{u} = 0 \,, \tag{28}$$

$$\nabla \cdot \mathbf{u} + \frac{p}{\rho_a c_a^2} = 0 \,. \tag{29}$$

Equations 28 and 29 correspond to the linearized Euler equation and the linear continuity equation, and by solving for $\mathbf{u}$ in Equation 28 and substituting it in Equation 29, one obtains the linear wave equation [12]. The former is used to ensure the kinematic compatibility between Ω_d and Ω_a. As it can be seen in Figure 1, some air elements are inserted between the wheel fairing and the coupling interface, in order not to catch possible numerical instabilities in the displacement field when large changes in material properties exist. Therefore the coupling boundary Γ_{coup} is placed in the air region, where both formulation are valid, thus easing the coupling process.

By evaluating the pressure gradient normal to the boundary Γ_{coup} in Equation 27, one obtains:

$$\frac{\partial p}{\partial n_p} = \mathbf{n}_p{}^T \nabla p = \mathbf{n}_p^T \left(\omega^2 \rho_a \mathbf{u} \right) \,, \tag{30}$$

and $\mathbf{F}_a$ results in:

$$\mathbf{F}_a^{coup} = \sum_{e=1}^{N_{coup}} \int_{\Gamma_e \cap \Gamma_{coup}} \mathbf{N}_p^T \mathbf{n}_p^T \left(\omega^2 \rho_a \mathbf{u} \right) \, \mathrm{d}\Gamma = \omega^2 \rho_a \sum_{e=1}^{N_{coup}} \int_{\Gamma_e \cap \Gamma_{coup}} \mathbf{N}_p^T \left(\mathbf{n}_p^T \mathbf{N}_u \right) \, \mathrm{d}\Gamma \, \tilde{\mathbf{U}} \,. \tag{31}$$

This term is then moved to the left-hand side of Equation 24 to create an additional mass term following the relation $\omega^2 \mathbf{M}_{ad}^{coup} = \mathbf{F}_a^{coup}$, obtaining:

$$\mathbf{M}_{ad}^{coup} = \rho_a \sum_{e=1}^{N_{coup}} \int_{\Gamma_e \cap \Gamma_{coup}} \mathbf{N}_p^T \left(\mathbf{n}_p^T \mathbf{N}_u \right) \, \mathrm{d}\Gamma \,. \tag{32}$$

On the other hand, the elastic equilibrium $\sigma \mathbf{n}_u = -p \mathbf{n}_u$ at Γ_{coup} is introduced into Equation 22 to obtain:

$$\mathbf{F}_a = \sum_{e=1}^{N_d} \int_{\Gamma_e \cap \Gamma_{coup}} \mathbf{N}_u^T \mathbf{n}_u \left(-\mathbf{N}_p \right) \, \mathrm{d}\Gamma \, \tilde{\mathbf{P}}_a \,. \tag{33}$$

Further manipulation leads to a new stiffness term in Equation 17:

$$\mathbf{K}_{da}^{coup} = \sum_{e=1}^{N_{coup}} \int_{\Gamma_e \cap \Gamma_{coup}} \mathbf{N}_u^T \mathbf{n}_u \mathbf{N}_p \, \mathrm{d}\Gamma \, . \tag{34}$$

The global system of equations obtained is:

$$\begin{bmatrix} \mathbf{K}_{uu} - \omega^2 \mathbf{M}_{uu} & \mathbf{C}_{up} & \mathbf{K}_{da}^{coup} \\ \mathbf{C}_{up}^T & \mathbf{D}_{pp} & 0 \\ -\omega^2 \mathbf{M}_{ad}^{coup} & 0 & \mathbf{K}_a - \omega^2 \mathbf{M}_a \end{bmatrix} \begin{bmatrix} \tilde{\mathbf{U}}_d \\ \tilde{\mathbf{P}}_d \\ \tilde{\mathbf{P}}_a \end{bmatrix} = \begin{bmatrix} \mathbf{F}_u \\ 0 \\ \mathbf{F}_a \end{bmatrix} \tag{35}$$

3. THE MULTI-OBJECTIVE OPTIMIZATION PROBLEM

As explained in Section 1, three objective functions f_k ($k = 1, 2, 3$) are treated in this paper. First, the vibro-acoustic analysis is considered and the integral of the acoustic pressure amplitude within Ω_i is to be minimized. Given a design point $\mathbf{x}$, this pressure integral $f_1(\mathbf{x})$ can be evaluated at a specific frequency or along a target frequency range $[\omega_0, \omega_1]$, in which case the mean value of $f_1(\mathbf{x})$ is calculated by means of a numerical integration quadrature. Second, the strain energy $f_2(\mathbf{x})$ of the structure when certain load cases are considered is also minimized in order to guarantee structural continuity. Finally, an additional penalty function is considered in order to force convergence of the n design variables x_e to either 0 (air) or 1 (solid). A polynomial function is defined, with $f_3(x_e) = -4x_e^2 + 4x_e$, so that $f_3(x_e)$ is maximum for intermediate values of x_e, and is zero for $x_e = 0$ and $x_e = 1$.

A linear scalarization of the aforementioned objective functions is considered in the present study. The resulting minimization problem, using the single-objective function $f_0(\mathbf{x})$ is:

$$\min_{\mathbf{x}} \quad f_0(\mathbf{x}) = \sum_{k=1}^{3} w_k f_k(\mathbf{x}) = w_1 \frac{\int_{\omega_0}^{\omega_1} \left(\int_{\Omega_i} \left| p(\mathbf{x}) \right| \, \mathrm{d}\Omega \right) \mathrm{d}\omega}{\omega_1 - \omega_0} + w_2 f_2(\mathbf{x}) + w_3 \sum_{e=1}^{n} f_3(x_e) \, , \tag{36}$$

$$\text{subject to} \quad 0 \leq x_e \leq 1 \quad \text{for } e = 1, ..., n \, . \tag{37}$$

Additionally, a number m of constraints $g_i(\mathbf{x})$ can be added in order to narrow the design space, such as the weight constraint, $g_1(\mathbf{x}) = W(\mathbf{x}) - W_0 \leq 0$, where W_0 is the desired weight and $W(\mathbf{x})$ is the weight of the structure at each iteration point:

$$g_i(\mathbf{x}) \leq 0 \quad \text{for } i = 1, ..., m \, . \tag{38}$$

The optimization problem is solved by the use of the iterative gradient-based Method of Moving Asymptotes (MMA) [16]. Given a design point $\mathbf{x}$, an approximation subproblem is generated, in which the objective function is replaced by the sum of several convex functions which are constructed using gradient information. The resolution of this subproblem is beyond the scope of this paper and the reader is referred to [16] for its description. The computation of the sensitivities of f_0 with respect to the design variables can be sped up (with respect to the finite difference method) by using the standard adjoint method [17], which is recalled in Section 4.

4. SENSITIVITY ANALYSIS

The standard adjoint method [17] is described below. Equation 35 is recalled here in compact form:

$$\mathbf{K}(\mathbf{x},\omega)\tilde{\mathbf{\Theta}}(\mathbf{x},\omega) = \mathbf{F}(\mathbf{x},\omega)\,, \tag{39}$$

where the column vector $\tilde{\mathbf{\Theta}}$ contains the displacement and pressure nodal values. At each iteration, for a certain frequency ω, the augmented objective function is defined as:

$$\widehat{f_0}\left(\tilde{\mathbf{\Theta}}(\mathbf{x})\right) = f_0\left(\tilde{\mathbf{\Theta}}(\mathbf{x})\right) - \boldsymbol{\lambda}^T(\mathbf{x})\left(\mathbf{K}(\mathbf{x})\tilde{\mathbf{\Theta}}(\mathbf{x}) - \mathbf{F}(\mathbf{x})\right) - \overline{\boldsymbol{\lambda}}^T(\mathbf{x})\left(\overline{\mathbf{K}(\mathbf{x})\tilde{\mathbf{\Theta}}(\mathbf{x}) - \mathbf{F}(\mathbf{x})}\right)\,, \tag{40}$$

$\boldsymbol{\lambda}(\mathbf{x})$ being the Lagrange multipliers column vector, and $\overline{(\cdot)}$ being the complex conjugate of $(\cdot)$. Differentiating previous expression with respect to the design variable x_e leads to:

$$\begin{aligned}\frac{\partial\widehat{f_0}}{\partial x_e} = &\left(\frac{\partial f_0}{\partial\tilde{\mathbf{\Theta}}_r}\right)^T\frac{\partial\tilde{\mathbf{\Theta}}_r}{\partial x_e} + \left(\frac{\partial f_0}{\partial\tilde{\mathbf{\Theta}}_i}\right)^T\frac{\partial\tilde{\mathbf{\Theta}}_i}{\partial x_e}\\ &- \boldsymbol{\lambda}^T\left(\frac{\partial\mathbf{K}}{\partial x_e}\tilde{\mathbf{\Theta}} + \mathbf{K}\left(\frac{\partial\tilde{\mathbf{\Theta}}_r}{\partial x_e} + j\frac{\partial\tilde{\mathbf{\Theta}}_i}{\partial x_e}\right) - \frac{\partial\mathbf{F}}{\partial x_e}\right)\\ &- \overline{\boldsymbol{\lambda}}^T\left(\overline{\frac{\partial\mathbf{K}}{\partial x_e}\tilde{\mathbf{\Theta}}} + \overline{\mathbf{K}}\left(\frac{\partial\tilde{\mathbf{\Theta}}_r}{\partial x_e} - j\frac{\partial\tilde{\mathbf{\Theta}}_i}{\partial x_e}\right) - \overline{\frac{\partial\mathbf{F}}{\partial x_e}}\right)\,,\end{aligned} \tag{41}$$

where the term $\dfrac{\partial\mathbf{K}}{\partial x_e}$ is derived analytically in order to save computation time. Column vectors $\dfrac{\partial f_0}{\partial\tilde{\mathbf{\Theta}}_r}$ and $\dfrac{\partial f_0}{\partial\tilde{\mathbf{\Theta}}_i}$ contain the derivatives of f_0 with respect to the real and imaginary parts of the nodal solution associated with the elements within Ω_i. Reordering the terms, the following expression is obtained:

$$\begin{aligned}\frac{\partial\widehat{f_0}}{\partial x_e} = &\left(\frac{\partial\tilde{\mathbf{\Theta}}_r}{\partial x_e}\right)^T\left(-\mathbf{K}^T\boldsymbol{\lambda} - \overline{\mathbf{K}^T\boldsymbol{\lambda}} + \frac{\partial f_0}{\partial\tilde{\mathbf{\Theta}}_r}\right)\\ &+ \left(\frac{\partial\tilde{\mathbf{\Theta}}_i}{\partial x_e}\right)^T\left(-j\mathbf{K}^T\boldsymbol{\lambda} + j\overline{\mathbf{K}^T\boldsymbol{\lambda}}\frac{\partial f_0}{\partial\tilde{\mathbf{\Theta}}_i}\right)\\ &- \boldsymbol{\lambda}^T\left(\frac{\partial\mathbf{K}}{\partial x_e}\tilde{\mathbf{\Theta}} - \frac{\partial\mathbf{F}}{\partial x_e}\right) - \overline{\boldsymbol{\lambda}}^T\left(\overline{\frac{\partial\mathbf{K}}{\partial x_e}\tilde{\mathbf{\Theta}} - \frac{\partial\mathbf{F}}{\partial x_e}}\right)\,.\end{aligned} \tag{42}$$

As the explicit form of the terms $\dfrac{\partial\tilde{\mathbf{\Theta}}_r}{\partial x_e}$ and $\dfrac{\partial\tilde{\mathbf{\Theta}}_i}{\partial x_e}$ is difficult to obtain, $\boldsymbol{\lambda}(\mathbf{x})$ is chosen so that:

$$-\mathbf{K}^T\boldsymbol{\lambda} - \overline{\mathbf{K}^T\boldsymbol{\lambda}} + \frac{\partial f_0}{\partial\tilde{\mathbf{\Theta}}_r} = 0\,, \tag{43}$$

$$-j\mathbf{K}^T\boldsymbol{\lambda} + j\overline{\mathbf{K}^T\boldsymbol{\lambda}} + \frac{\partial f_0}{\partial\tilde{\mathbf{\Theta}}_i} = 0\,. \tag{44}$$

Multiplying Eq. 44 by $-j$ and adding Eq. 43 leads to [17]:

$$\boldsymbol{\lambda} = \frac{1}{2}\left(\mathbf{K}^T(\mathbf{x})\right)^{-1}\left(\frac{\partial f_0}{\partial\tilde{\mathbf{\Theta}}_r} - j\frac{\partial f_0}{\partial\tilde{\mathbf{\Theta}}_i}\right)\,. \tag{45}$$

Finally, the sensitivity of the objective function with respect to each design variable x_e is calculated as [17]:

$$\frac{\partial \widehat{f_0}}{\partial x_e} = -2\Re\left\{\boldsymbol{\lambda}^T\left(\frac{\partial \mathbf{K}}{\partial x_e}\tilde{\boldsymbol{\Theta}} - \frac{\partial \mathbf{F}}{\partial x_e}\right)\right\} \quad \text{for } e = 1, ..., n\,, \tag{46}$$

where $\Re\{(\cdot)\}$ is the real part of the complex $(\cdot)$.

5. EXAMPLE OF BOGIE FAIRING TOPOLOGY OPTIMIZATION FOR ROLLING NOISE MINIMIZATION AT A GIVEN FREQUENCY

In this section, a fairing is optimized in order to minimize the rolling noise perceived in the surroundings. The case study is modelled in 2D for the validation of the aforementioned optimization method. The frequency of study is set to 800 Hz. Neumann boundary conditions are applied at Γ_{rad} in order to model the wheel vibration by means of an input displacement normal to the boundary. The absorbing boundary Γ_{abs} is modelled by applying the Sommerfeld condition $\mathbf{n}\cdot\nabla p + ikp = 0$ [12], evaluated in Equation 27.

All design variables x_e are initially set to 0.5, as seen in Figure 2a. The objective function coefficients are $w_1 = 1$, $w_2 = 0.1$ and $w_3 = 0.3$. For the present analysis, $c_a = 340$ m/s, $\rho_a = 1.225$ kg/m^2, $E = 3.5$ GPa, $\nu = 0.34$ and $\rho_s = 1320$ kg/m^2. The pressure integral whithin the receiver area is $f_1^{(0)} = 7.4351$ N, whereas the initial compliance of the structure under the aforementioned load case is $f_2^{(0)} = 9.3287$ mJ.

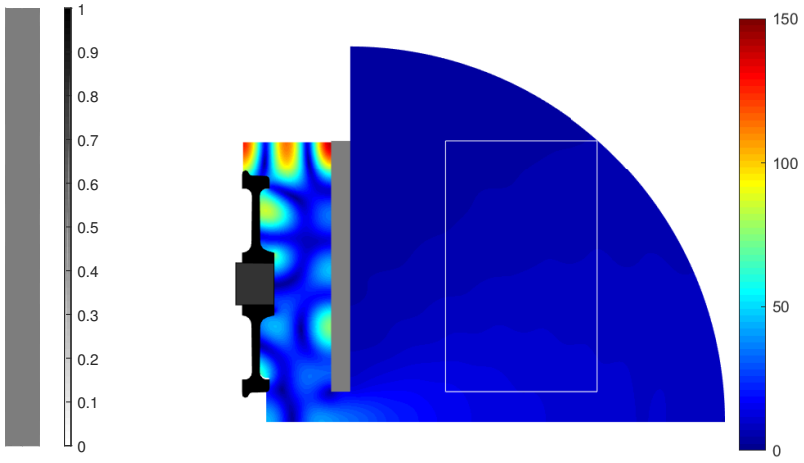

(a) Topology $x_e^{(0)}$ *(b) Acoustic field $|p|$ in Pa*

Figure 2: Initial problem

A traction pressure in the lower surface is considered in this case study. As it can be seen in Figure 3a, the optimized topology after 46 iterations includes several voids within the structure. The resulting acoustic pressure field is shown in Figure 3b. Significant noise reduction in the surroundings is observed. The pressure amplitude integral decreases to $f_1^{(73)} = 5.7696$ N. The strain energy slightly decreased to $f_2^{(73)} = 9.1949$ mJ, due to the lower weighing coefficient of this objective function, $w_2 << w_1$. Additionally, the weight constraint is fulfilled.

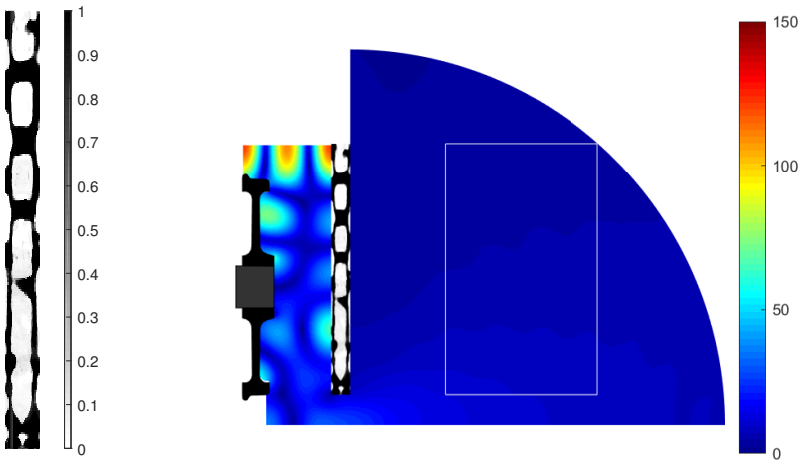

(a) Topology $x_e^{(46)}$ *(b) Acoustic field |p| in Pa*

Figure 3: Final problem

Next, the difference in wave pressure amplitude, $\left|p^{(46)}\right| - \left|p^{(0)}\right|$ is shown within Ω_i. A mean decrease of about 1.6 Pa is observed for the final design with respect to the initial one within the target area.

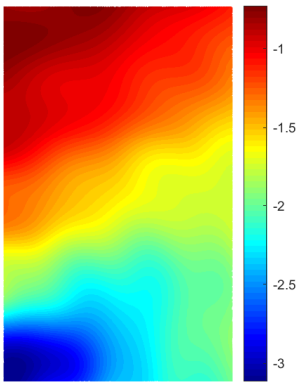

Figure 4: Diference in acoustic pressure absolute value, $\left|p^{(46)}\right| - \left|p^{(0)}\right|$

6. CONCLUSIONS

A TO scheme with reduced computational cost for the coupled vibro-acoustic problem has been set up through the use of the domain decomposition technique, by implementing the mixed u/p formulation in a small region of the problem domain, while solving the Helmholtz equation in the rest of the air region. The optimization problem is solved by the iterative gradient-based solver MMA.

The use of the adjoint method, along with the analytical derivation of the global matrices with respect to each design variable, allows to efficiently calculate the sensitivities of the objective function.

The results show a considerable improvement in the acoustic performance of the optimized wheel fairing with respect to the initial topology. The additional consideration of the compliance minimization problem under a static load case makes the design achieved to be structurally continuous.

Future works will focus on the consideration of variable-dependant volumetric forces in the static analysis and the design of sound barriers under maximum admissible elastic stress restrictions.

7. ACKNOWLEDGEMENTS

The authors gratefully acknowledge the financial support of Ministerio de Ciencia, Innovación y Universidades–Agencia Estatal de Investigación and the European Regional Development Fund (projects TRA2017-84701-R and DPI2017-89816-R), as well as Generalitat Valenciana (project Prometeo/2016/007).

8. REFERENCES

[1] Martin P. Bendsøe. *Optimization of Structural Topology, Shape, and Material*. Springer, 1995.

[2] Ole Sigmund. A 99 line topology optimization code written in matlab. *Struct. Multidiscip. Optim.*, 21(2):120–127, 2001.

[3] Eddie Wadbro and Martin Berggren. Topology optimization of an acoustic horn. *Comput. Methods Appl. Mech. Eng.*, 196(1-3):420–436, 2006.

[4] Maria B. Dühring, Jakob S. Jensen, and Ole Sigmund. Acoustic design by topology optimization. *J. Sound Vib.*, 317(3-5):557–575, 2008.

[5] Ki Hyun Kim and Gil Ho Yoon. Optimal rigid and porous material distributions for noise barrier by acoustic topology optimization. *J. Sound Vib.*, 339:123–142, 2015.

[6] Jianhui Luo and Hae Chang Gea. Optimal Stiffener Design for Interior Sound Reduction Using a Topology Optimization Based Approach. *J. Vib. Acoust.*, 125(3):267, 2003.

[7] Jianbin Du and Niels Olhoff. Minimization of sound radiation from vibrating bi-material structures using topology optimization. *Struct. Multidiscip. Optim.*, 33(4-5):305–321, 2007.

[8] Morten Birkmose Søndergaard and Claus B.W. Pedersen. Applied topology optimization of vibro-acoustic hearing instrument models. *J. Sound Vib.*, 333(3):683–692, 2014.

[9] Lei Shu, Michael Yu Wang, Zongde Fang, Zhengdong Ma, and Peng Wei. Level set based structural topology optimization for minimizing frequency response. *J. Sound Vib.*, 330(24):5820–5834, 2011.

[10] Renato Picelli, William Martins Vicente, and Renato Pavanello. Evolutionary topology optimization for structural compliance minimization considering design-dependent FSI loads. *Finite Elem. Anal. Des.*, 135:44–55, 2017.

[11] Ole Sigmund and Peter Michael Clausen. Topology optimization using a mixed formulation: An alternative way to solve pressure load problems. *Comput. Methods Appl. Mech. Eng.*, 196(13-16):1874–1889, 2007.

[12] Gil Ho Yoon, Jakob Søndergaard Jensen, and Ole Sigmund. Topology optimization of acoustic-structure interaction problems using a mixed finite element formulation. *Int. J. Numer. Methods Eng.*, 70(9):1049–1075, 2007.

[13] Klaus-Jürgen Bathe. Finite Element Procedures. In *Prentice Hall, Inc.*, chapter 4.4, page 1073. K.J. Bathe, Watertown, MA, second edition, 1996.

[14] Jorge Gutiérrez-Gil, Xavier Garcia-Andrés, José Martínez-Casas, Enrique Nadal, and Francisco David Denia. Mitigation of Railway Wheel Rolling Noise by Using Advanced Optimization Techniques. In *EngOpt 2018 Proc. 6th Int. Conf. Eng. Optim.*, pages 1141–1153. Springer International Publishing, Cham, 2019.

[15] Lawrence E. Kinsler. *Fundamentals of acoustics*. Wiley, 2000.

[16] Krister Svanberg. The method of moving asymptotes—a new method for structural optimization. *Int. J. Numer. Methods Eng.*, 24(2):359–373, 1987.

[17] Jakob S. Jensen. Topology optimization. In *CISM Int. Cent. Mech. Sci. Courses Lect.*, volume 540, pages 109–159. Springer Vienna, Vienna, 2012.